Proteoglycan Research

WILEY

Proteoglycan Research

ORIGINAL RESEARCH OPEN ACCESS

A Circular Economy Strategy for Repurposing Heparin Manufacturing By-Products as Anti-Inflammatory Therapeutics

Emilia Uslenghi[1] | Taran Kandola[2] | Sofia Nizzolo[1] | Ethan Saunders[2] | Tye Gee Jun[3,4] | Mark A. Skidmore[2] | Edwin A. Yates[5] | Marco Guerrini[1] | Marcelo A. Lima[2] | Antonella Bisio[1]

[1]Istituto di Ricerche Chimiche e Biochimiche G. Ronzoni, Milan, Italy | [2]Centre for Glycoscience, School of Life Sciences, Keele University, Keele, UK | [3]Institute for Research in Molecular Medicine (INFORMM), Universiti Sains Malaysia (USM), Minden, Pulau Pinang, Malaysia | [4]Malaysian Institute of Pharmaceuticals and Nutraceuticals, National Institutes of Biotechnology Malaysia, Gelugor, Pulau Pinang, Malaysia | [5]Department of Biochemistry and Systems Biology, Institute of Systems, Molecular and Integrative Biology, University of Liverpool, Liverpool, UK

Correspondence: Marcelo A. Lima (m.andrade.de.lima@keele.ac.uk) | Antonella Bisio (bisio@ronzoni.it)

Received: 31 March 2025 | **Revised:** 11 June 2025 | **Accepted:** 27 June 2025

Funding: This study was supported by the Royal Society (IEC\NSFC\201116), the Academy of Medical Sciences/Wellcome Trust (Springboard grant, SBF007\100054), EPSRC (EP/X019179/1), and Ronzoni Foundation.

ABSTRACT

Heparin manufacturing generates significant volumes of by-products, which are typically treated as waste, and whose potential as a source of alternative bioactive materials is yet to be fully developed. Here, we employed a circular economy approach to support the repurposing of this waste stream for potential anti-inflammatory applications. Glycosaminoglycan fractions were extracted and purified from porcine-derived heparin by-products and structurally characterised using nuclear magnetic resonance and high performance size exclusion chromatography. The fractions exhibited distinct saccharide compositions, sulfation patterns, and molecular weight profiles. Bioactivity assays demonstrated that selected fractions attenuated LPS-induced NF-κB activation in RAW-Blue™ cells and enhanced IL-10 production ex vivo, indicating immunomodulatory potential. Heparin by-products have negligible anticoagulant activity, which supports their safe use in non-anticoagulant biomedical applications. These findings illustrate the potential of heparin by-products as therapeutic agents, while contributing to sustainable pharmaceutical manufacturing.

1 | Introduction

Several recent and emerging challenges make the effective use of existing bioactive materials for medical purposes an urgent priority. The COVID-19 pandemic highlighted the unpreparedness of global health systems to rapidly address developing medical challenges. More recently, the geopolitical uncertainty stemming from irresponsible government actions, the scarcity of resources, conflicts, and climate change have also illustrated the fragility of supply chains, which are already under strain from inexorably growing demand [1]. Bioactive materials that are already produced but, not fully utilised, offer an attractive reservoir with the potential to serve various roles, including as pharmaceuticals. However, the useful activities that these materials may harbour have largely remained unexplored.

Heparin, a highly sulfated glycosaminoglycan (GAG), is critical in anticoagulation therapy. Structurally, its main repeating disaccharide unit is α-D-glucosamine N,6-sulphate (GlcNS,6S) linked 1,4 to α-L-iduronic acid 2-O-sulphate (IdoA2S) [2], yet variable substitution patterns occur, contributing to its strong interaction with proteins such as antithrombin (AT) [3]. By potentiating the inhibitory activity of AT on thrombin and other

serine proteases in the coagulation cascade, heparin is an essential therapeutic agent for preventing and treating thromboembolic disorders [4]. Beyond its well-established anticoagulant function, heparin exerts additional biological effects, including anti-inflammatory [5], antiviral [6, 7], and antitumor activities [8], mediated through its ability to interact with cytokines, adhesion molecules, and immune cells [9].

The large-scale extraction of pharmaceutical unfractionated heparin (UFH) from porcine intestinal mucosa generates significant quantities of structurally related GAGs and heparin fractions with lower anticoagulant potency [10]. GAGs exhibit redundancy between substitution patterns and bioactivity, providing them with the unique property that several distinct structures can elicit a particular activity, which, in turn, enables the use of GAGs from a variety of sources. Since there are potentially many active structures, those with favourable on-target activities and minimal side effects can be selected.

Materials that retain desirable bioactive properties therefore hold the potential for repurposing in non-anticoagulant biomedical applications [11]. This presents an opportunity to diversify the use of heparin-derived materials while adding value to its manufacturing waste products.

The valorisation of heparin manufacturing by-products aligns with the principles of the circular economy, directly supporting the United Nations Sustainable Development Goals (SDGs) [12]. Transforming heparin production waste streams into valuable bioactive compounds can promote sustainability in biomedical manufacturing, reduce dependency on primary resources, and minimises environmental impact [13]. Furthermore, deploying such an approach will address global challenges associated with the ethical sourcing of animal-derived materials and the need for sustainable innovation in drug development aimed at improved resource efficiency and industrial resilience.

We set out to survey the side-product fractions generated during pharmaceutical heparin manufacture, focusing on establishing their basic anti-inflammatory properties while also considering their anticoagulant potential. We employed orthogonal analytical methodologies to elucidate their molecular composition, followed by functional assays using RAW-Blue™ cells [14], a murine macrophage reporter cell line, and peripheral blood mononuclear cells (PBMCs). The results contribute to the growing body of evidence supporting the multifaceted application of heparin-derived compounds, facilitating a transition toward a more sustainable and innovation-driven heparin manufacturing industry.

2 | Materials and Methods

2.1 | Heparin By-Product Isolation and Structural Characterisation

Crude material was sourced from Chenzhong Biopharma, Shangdong, China. Two crude by-product fractions (ca. 5 g samples of each were supplied) were isolated from 1800 porcine intestinal mucosa specimens as previously described [10]. Briefly, the original process involved treatment with protease enzymes and anion exchange chromatography. The first fraction was eluted and precipitated with ethanol before drying, yielding fraction FI, 0.5 kg. The solution from this step underwent a second round of purification, involving repeating stages of anion exchange chromatography and ethanol precipitation to yield fraction FII, 0.25 kg.

Samples were further fractionated by Ion Exchange Chromatography (IEC) using a DEAE-Sephacel column (2.6 × 35 cm). A total of 1.2 g of the sample was loaded onto the column, and separation was carried out using a stepwise NaCl gradient. Elution was performed at a flow rate of 1.5 mL/min. The NaCl gradient ranged from 0.0 M to 2.0 M, and seven fractions of 200 mL each were collected. The fraction distribution and respective NaCl concentrations were as follows: Fraction 1 (0.2 M), Fraction 2 (0.4 M), Fraction 3 (0.6 M), Fraction 4 (0.8 M), Fraction 5 (1.0 M), and Fraction 6 (1.2 M), with Fraction 7 eluted at 2.0 M NaCl. All fractions were thoroughly desalted using a 2 KDa cut-off membrane dialysis.

Size exclusion chromatography (SEC) was further deployed to generate size-defined fractions using a Superdex S75 (3 × 87 cm) column coupled to a fast protein liquid chromatography (FPLC) system. A total of 250 mg of sample was loaded onto the column, with elution carried out using 0.25 M NH_4Cl as the mobile phase. The flow rate was maintained at 5 mL/min, and elution was monitored at UV 210 nm. Fractions were collected based on elution time windows and analysed for the yield of FI and FII. The major elution peaks were observed within specific retention times, with fractions labelled A to F. The time window (in minutes) for each fraction was 37-51 (A), 51-65 (B), 65-79 (C), 79-93 (D), 93-107 (E), and 107-142 (F). Fractions were pooled based on molecular weight distribution and further processed for downstream applications.

2.2 | Nuclear Magnetic Resonance (NMR) Spectroscopy

1D NMR spectra were acquired using a Bruker AVANCE III 600 MHz spectrometer (Karlsruhe, Germany) equipped with a TCI 5 mm cryogenic probe. The experiments were performed at 298 K with a constant presaturation power of 7 Hz. The acquisition parameters were set as follows: 32 scans, 8 dummy scans, a relaxation delay of 12 s, a spectral width of 18 ppm, and a transmitter offset of 4.7 ppm. Data processing involved exponential multiplication with a line broadening of 0.3 Hz, followed by Fourier transformation, phase correction, baseline correction, and calibration against the TSP signal. Two-dimensional $^{1}H/^{13}C$-HSQC spectra were recorded using either a Bruker AVANCE III 600 MHz spectrometer or a Bruker AVANCE III HD 500 MHz spectrometer (Karlsruhe, Germany), both equipped with TCI 5 mm cryogenic probes. The Bruker library hsqcetgpsisp2.2 pulse sequence was used for data acquisition at 298 K. The experiments were acquired with 24 scans, 16 dummy scans, and a relaxation delay of 2.5 s for the 600 MHz spectrometer, while the 500 MHz spectrometer used 40 scans, 16 dummy scans, and a relaxation delay of 2 s. The spectral width was set to 8 ppm for F2 and 80 ppm for F1, with transmitter offsets of 4.7 ppm and 80 ppm for F2 and F1, respectively. The 1JC-H coupling constant was fixed at 150 Hz. Data processing involved zero filling to 4k points in F2, linear prediction to 640

points with zero filling to 1k in F1, and apodisation using a 90°-shifted squared sine bell function in both dimensions. Spectral processing and integration were performed using TopSpin software (version 3.5, Bruker BioSpin, Rheinstetten, Germany) [15, 16].

2.3 | High Performance Size Exclusion Chromatography Combined With a Triple Detector Array (HP-SEC/TDA)

The HPLC system comprised a Viscotek system (Malvern Instrument Ltd, Malvern, UK) equipped with a VE1121 Solvent Delivery pump and a Gastorr 150 metal-free two-channel online degassing device. The detector system was a Viscotek Model 302 Triple Detector Array, which was configured as previously described [17], with the addition of a Low Angle Laser Light Scattering (LALLS) detector. The LALLS detector operated at measuring angles of 90° and 7°, using a constant optical power output laser diode as the light source, with a wavelength of 670 nm. The detection system consisted of a photodiode/amplifier setup with a cell volume of 10 μL.

Chromatographic separation was performed using two TSK gel columns in series, G3000 PWXL (7.8 × 300 mm) and G2500 PWXL (7.8 × 300 mm) (Tosoh Corp., Tokyo, Japan). The columns, injector, and detectors were maintained at a constant temperature of 40°C. The mobile phase consisted of an aqueous 0.1 M $NaNO_3$ solution, pre-filtered through a 0.22 μm filter (Merck Millipore, Darmstadt, Germany), and was delivered at a flow rate of 0.6 mL/min. The system was calibrated using a polyethylene oxide (PEO) narrow standard with known molecular weight (Mw), polydispersity, and intrinsic viscosity.

Data analysis was conducted using OmniSEC software, version 4.0 (Viscotek). A differential refractive index increment ($d\eta/dc$) value of 0.120 was applied to convert refractive index (RI) voltages into solute concentration at each data slice across the chromatographic peak [17].

2.4 | RAW-Blue™ Cells Assay

The RAW-Blue™ cell line, derived from murine RAW 264.7 macrophages, was used to assess NF-κB and alkaline phosphatase (AP) production in response to pattern recognition receptor (PRR) stimulation. These cells stably express an inducible secreted embryonic alkaline phosphatase (SEAP) reporter gene, making them an effective model for monitoring inflammatory responses triggered by LPS stimulation. SEAP activity in the supernatant was measured using QUANTI-Blue™ Solution, a SEAP detection medium that provides a direct readout of NF-κB/AP activation levels.

To investigate the impact of heparin by-product fractions on LPS-induced NF-κB/AP activation, RAW-Blue™ cells were seeded into 96-well plates at a density of ~100,000 cells per well in a final volume of 200 μL. Cells were stimulated with 20 μL of LPS (10 ng/mL final concentration) and with (100 μg/mL final concentration) or without by-product fractions, with appropriate controls included. The plate was incubated at 37°C in a 5% CO_2 incubator for 18–24 h. After incubation, 20 μL of cell culture supernatant was transferred to a new well containing 180 μL of QUANTI-Blue™ Solution and incubated at 37°C for 30 to 4 h to allow colour development. Optical density (OD) was measured at 620–655 nm at time points ranging from 0.5 to 4 h using a microplate reader.

2.5 | Peripheral Blood Mononuclear Cells (PBMCs) Ex Vivo Assay

Whole blood was collected in anticoagulant-treated tubes (EDTA blood collection tubes) and diluted with an equal volume of Dulbecco's Phosphate Buffered Saline (DPBS). Ficoll-Paque was shaken thoroughly before use, and 3 mL was carefully layered into centrifuge tubes. Diluted blood (4 mL) was gently layered on top of the Ficoll-Paque without mixing, maintaining distinct phases. Density gradient centrifugation was performed at 400 × g for 30–40 min at 18°–20°C using a swing-bucket rotor, ensuring minimal disruption of the separation layers by turning the brakes off.

Following centrifugation, the upper plasma layer was carefully removed using a pipette without disturbing the underlying layers. The mononuclear cell layer was then carefully transferred to a fresh tube, avoiding contamination from the lower Ficoll layer. The isolated PBMCs were washed by adding three volumes of DPBS and gently mixed before centrifugation at 400 × g for 10–15 min at 18°–20°C. An additional wash step was performed at a reduced centrifugation speed of 60–100 × g to further remove platelets. The supernatant was discarded, and the washing step was repeated using the same volume of DPBS. The final PBMC pellet was resuspended in RPMI supplemented with foetal bovine serum (FBS) and 1% Penicillin-Streptomycin (Pen-Strep) to a final volume of 1 mL for subsequent cell culture and stimulation assays.

Purified PBMCs were resuspended in RPMI containing 10% FBS and 1% Pen-Strep at a final concentration of 2×10^6 cells/mL. A total of 100 μL of the PBMC suspension, corresponding to 2×10^5 cells per well, was added to a 96-well plate. Immune stimulation was carried out by adding 20 μg of heparin and heparin by-product fractions per well, with a final concentration of 100 μg/mL. Phorbol 12-myristate 13-acetate (PMA) and ionomycin (2 μL/mL) were added for positive controls, while media-only wells served as negative controls [18]. All conditions were tested in triplicate. Control wells containing only PBMCs were included to assess baseline responses.

Plates were incubated at 37°C in a 5% CO_2 incubator for 72–84 h, allowing for sufficient immune activation over the weekend. Following incubation, supernatants were collected for downstream analyses to evaluate IL-10 production using ELISA MAX™ Deluxe Set (Biolegend, UK) following manufacturers' instructions.

3 | Results

3.1 | Initial Purification and Recovery

By-products from the production of pharmaceutical heparin were processed to isolate GAGs. Following anion exchange chromatography and ethanol precipitation, the initial extraction

yielded approximately 0.5 kg of material, FI. Another fraction of 0.25, FII, kg was obtained after a second round of anion chromatography and ethanol precipitation.

3.2 | Structural Characterisation of Heparin-By-Products Precursors

The two samples were initially subjected to Mw analysis utilising HP-SEC/TDA. FI (Table 1) and FII (Table 2) presented similar Mw values of 25500 Da and 24500 Da, respectively; the polydispersity of both samples was calculated, and they were 1.45 and 1.48, respectively (Table S1). Mw values are higher than what is commonly observed in pharmaceutical heparin samples, while the polydispersity values are indicative of polydisperse GAG populations typical of naturally occurring polysaccharides. The molecular weight distribution parameters of the precursor fractions are detailed in (Table S1**)**.

Partial structural elucidation was first achieved by applying ^{1}H-NMR and ^{13}C-NMR spectroscopy (Figure 1), which revealed characteristic chemical shifts that enabled the identification of specific proton and carbon environments within the sugar residues corresponding to the saccharide backbone. The combined spectral data confirmed the presence of complex GAG mixtures, revealing variations in the monosaccharide composition and linkage patterns across different fractions. Traces of nucleic acids were also detected in both FI and FII spectra. Both samples were also subjected to 2D NMR (^{1}H/^{13}C HSQC), which suffers from less signal overlap (Figures S6 and S7), enabling detailed monosaccharide composition and determination of the degree of sulfation for each sample. The relative distribution of heparin/heparan sulphate (HP/HS), dermatan sulphate (DS), and chondroitin sulphate (CS) within each fraction were determined (Tables 2 and 3). Fraction FII exhibited a slightly higher proportion of HP/HS (60.8%) compared to FI (57.7%), while DS content was slightly lower in FII (25.3%) than in FI (27.1%). CS levels were similar between the two samples, ranging from 13.9% to 15.2%. The overall degree of sulfation, a critical determinant of biological activity, was also slightly higher in FII (1.71) than in FI (1.64).

Further differentiation of glucosamine residues linked to different uronic acids (IdoA, GlcA) provided additional structural insights. Both samples presented values for 3-O-sulfated glucosamine (A*), especially GlcA linked to A* (G-A*), a marker for anticoagulant activity, below the detection level (Table S2). The relative composition of uronic acids was also investigated. IdoA2S was the predominant uronic acid species in both fractions, accounting for ~50% of total uronic acid content. GlcA levels were higher in FI (36.9%) compared to FII (32.0%), whereas IdoA2OH was consistent in both samples (12.9%). Minor components such as 2,3-epoxide-modified uronic acids and GalA were below detection limits in both fractions, and the presence of GlcA2S was also undetected in either sample (Tables S2 and S3).

Together, the NMR data confirmed that both FI and FII were highly sulfated GAGs with distinct, yet comparable, compositional profiles. The relatively higher HP/HS content in FII suggests a closer resemblance to heparin-like structures, whereas FI contained a slightly greater proportion of DS and CS. As a result of the overall composition analysis, the disaccharide sulfation degree of the two precursors appeared slightly lower for FI (1.64) compared to FII (1.71).

TABLE 1 | Yield of fractions obtained from FI and FII by IEC and SEC.

Fraction	IEC NaCl (M)	SEC retention time (min)	FI (mg)	FII (mg)
1	0.2		2.1	3.4
2	0.4		81.6	33.8
3	0.6		634.4	594.7
4	0.8		286.5	113.6
5	1.0		7.5	1.5
A		37–51	121.4	151.5
B		51–65	207.6	205.7
C		65–79	60.8	71.5
D		79–93	29.0	26.5
E		93–107	46.7	30.7
F		107–142	13.8	3.6

3.3 | Further Charge and Size Fractionation of Precursors

The precursor heparin production by-products FI and FII were further fractionated utilising IEC and SEC to eliminate all residual non-GAG species, such as nucleic acids and possibly peptides resulting from protease digestion, and to reduce the complexity of

TABLE 2 | Molecular weight and composition of FI fractions.

	Fraction	HP/HS (%)	DS (%)	CS (%)	Degree of sulfation	Mw (kDa)
	FI	57.7	27.1	15.2	1.64	25.5
IEC fractionation	FI-3	65.8	20.6	13.6	1.49	23.2
	FI-4	35.2	38.4	26.4	2.21	26.0
SEC fractionation	FI-A	39.2	36.8	23.9	1.11	34.7
	FI-B	55.7	25.6	18.7	1.52	21.9
	FI-C	87.7	8.0	4.3	1.92	7.2

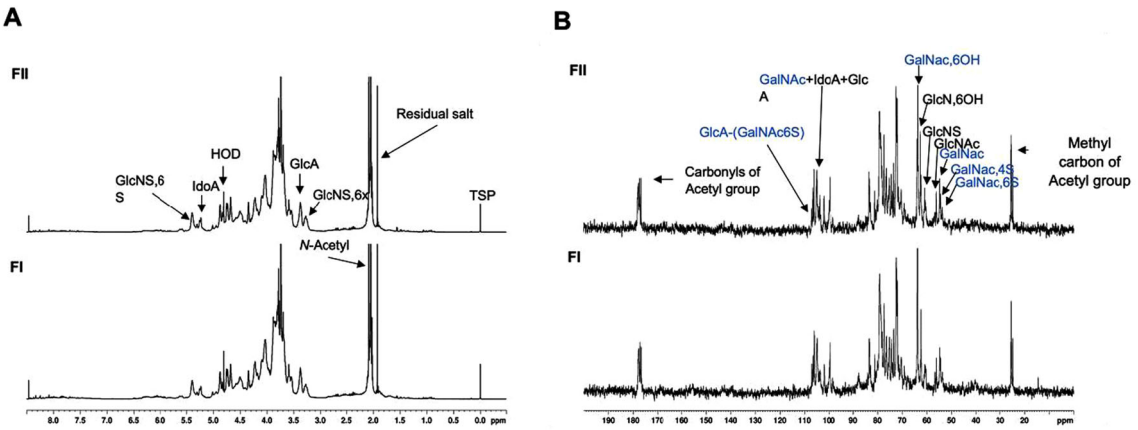

FIGURE 1 | ^{1}H (A) and ^{13}C NMR (B) spectra of heparin byproduct precursor fractions. Main peaks associated with GAG type and substitution pattern are assigned. Glc, glucosamine; GalNAc, N-acetyl galactosamine; S, sulphate; IdoA, iduronic acid; GlcA, glucuronic acid; HOD, residual HDO; TSP, trimethylsilylpropanoic acid; x stands for sulphate or hydroxyl group.

TABLE 3 | Molecular weight and composition of FII fractions.

	Fraction	HP/HS (%)	DS (%)	CS (%)	Degree of sulfation	Mw (kDa)
	FII	67.5	25.3	13.9	1.71	24.5
IEC fractionation	FII-3	65.0	21.9	13.1	1.84	22.2
	FII-4	22.8	44.8	32.4	2.30	26.0
SEC fractionation	FII-A	42.2	35.1	22.7	1.18	34.3
	FII-B	62.0	22.3	15.7	1.62	20.8
	FII-C	84.2	10.4	5.4	1.99	7.2

the samples for in-depth structural analysis. A total of 1.2 g of sample was loaded onto the DEAE-Sephacel column for each run, and fractions were eluted using a NaCl gradient ranging from 0.2 M to 2.0 M. The yield of IEC fractionations for FI and FII precursors is reported in Table 1. The results demonstrate that the majority of GAGs were efficiently separated between 0.4 M and 1.0 M NaCl, with the highest proportion eluting at 0.6 M NaCl. This suggests that the primary GAG species in both FI and FII exhibit similar total charge density, although differences in recovery at higher salt concentrations indicate some degree of heterogeneity in charge distribution.

In parallel, FI and FII fractions were also subjected to size exclusion chromatography (SEC) using a Superdex S75 column. The SEC chromatograms for FI and FII revealed slightly distinct elution patterns, with multiple fractions being collected at specific time intervals (Figure S1). The presence of material in lower molecular weight fractions suggested a degree of heterogeneity, possibly arising from minor degradation products or natural variations in GAG chain length. The yield of SEC fractionations for FI and FII precursors is reported in Table 1.

3.4 | Structural Characterisation of Charge and Size Defined Heparin Production By-Products

NMR spectroscopy was employed to characterise the fractions obtained from IEC and SEC, providing detailed insights into their disaccharide composition, sulfation patterns, and structural features. First, ^{1}H and $^{1}H/^{13}C$ NMR profiles of all the isolated fractions were analysed to evaluate the degree of purification of GAG structures. Representative spectra are presented in Figure 2, S8 and S9. Regarding the fractions isolated by IEC, FI-3, FI-4, FI-5, and similarly FII-3, FII-4, and FII-5 exhibited substantially purified GAG profiles, while the fractions FI-1 and FI-2, along with FII-1 and FII-2, appeared to be composed exclusively or mainly of non-GAG structures. These latter fractions turned out to be primarily nucleic acid degradation products, as they were abundantly present abundantly in fractions D and E isolated by SEC from both FI and FII. In fact, as shown in Figures S2–S5, the ^{1}H-NMR profiles of fractions A, B, and C of both precursors correspond to a highly purified GAG mixture, whose components (HP/HS, DS, and CS) are expected to be present in different proportion.

Based on these results, fractions 3 and 4, along with fractions A, B, and C from both precursors, were selected for further structural investigation. Fractions FI-5 and FII-5 were not considered owing to their limited quantity (Table 1). HSQC analyses were performed on the selected fractions to determine the relative content of HP/HS, DS, and CS (Tables 1 and 2).

For the IEC fractions, FI-3 and FII-3 showed the highest HP/HS content (65.8% and 65.0%, respectively). In contrast, DS and CS were most prevalent in FI-4 (38.4% and 26.4%, respectively) and particularly in FII-4 (44.8% and 32.4%, respectively). The overall sulfation degrees were 1.49 and 2.21 for FI-3 and FI-4 fractions, while they were 1.84 and 2.30 for FII-3 and FII-4. These

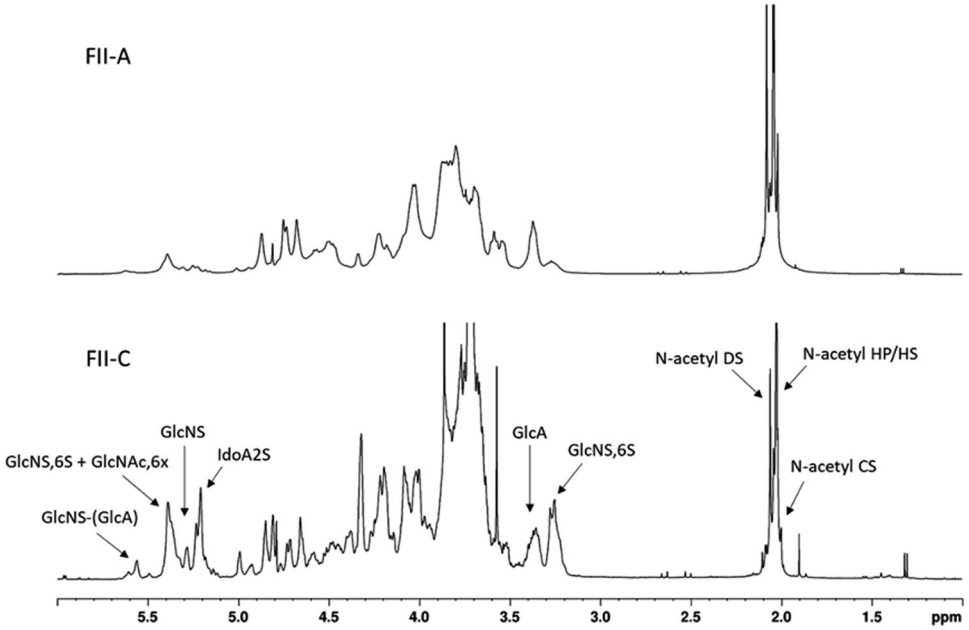

FIGURE 2 | Representative ^{1}H (A) NMR spectra of heparin byproduct fraction (FII-A and FII-C). Main peaks associated with GAG type and substitution patterns are assigned. DS, dermatan sulphate; CS, chondroitin sulphate; HP, heparin; HS, heparan sulphate; Glc, glucosamine; GalNAc, N-acetyl galactosamine; S, sulphate; IdoA, iduronic acid; GlcA, glucuronic acid; x stands for sulphate or hydroxyl group.

findings illustrate that IEC effectively separated GAGs based on their sulfation patterns and disaccharide composition.

For the SEC fractions, a similar trend was observed, with NMR analysis revealing a progressive enrichment of HP/HS and a decrease in DS and CS content from FI-A to FI-C. FI-A contained the highest DS (36.8%) and CS (23.9%) content, while FI-C and FI-D were almost entirely composed of HP/HS (> 80%). The degree of sulfation increased across the SEC fractions, ranging from 1.11 in FI-A to 1.92 in FI-C, indicating a greater abundance of highly sulfated disaccharides in later-eluting fractions.

A similar pattern was observed in FII samples, where HP/HS content increased progressively, while DS and CS content decreased. FII-A contained a lower proportion of HP/HS (~42%) and higher DS (~35%) and CS (~22%), whereas FII-C was highly enriched in HP/HS (~84%), with only minor contributions from DS (~10%) and CS (~5%). This shift in composition corresponded to an increase in sulfation degree, ranging from 1.18 in FII-A to 1.99 in FII-C, showing an increased sulfation density within later-eluting fractions.

Fractions were further analysed using HP-SEC/TDA (Table 1 and S1). For the IEC fractions, FI-3 and FII-3 contained the smallest GAG species (Mw 23.2 kDa and 22.2 kDa, respectively), with broad polydispersity indexes (1.72 and 1.62, respectively), whereas fractions FI-4 and FII-4 were composed of slightly higher molecular weight species (26.0 kDa) and reduced polydispersity (1.25). For the SEC fractions, the HP-SEC/TDA analysis confirmed distinct molecular weight differences among the samples, showing decreasing molecular weight distribution from FI-A to FI-C. In particular, FI-A exhibited the largest molecular weight species (Mw 34.7 kDa), while FI-C contained the smallest primary peak (Mw~7.2 kDa). The polydispersity index (Mw/Mn) ranged from 1.05 to 1.26, indicating that all fractions were relatively homogeneous. A similar trend was displayed by the FII fractions; FII-A containing larger GAG species (Mw 34.3 kDa) and FII-C exhibiting a significantly lower Mw of 7.2 kDa and a reduced polydispersity value of 1.05, accounting for a homogeneous peak of short-chain GAGs.

The combined NMR and molecular weight analyses confirmed that both IEC and SEC fractionation strategies effectively separated GAGs based on their degree of sulfation, disaccharide composition, and molecular size. Later-eluting fractions (FI-C and FII-C) were primarily composed of low molecular weight HP/HS, featuring greater abundance of highly sulfated IdoA2S-containing structures, leading to higher degrees of sulfation. In contrast, earlier fractions (FI-A, FI-B, FII-A, and FII-B) contained a more heterogeneous mixture of high molecular weight HP/HS, DS, and CS. These structural variations are anticipated to influence biological activity, particularly regarding protein interactions and inflammatory modulation, which were further investigated in subsequent assays.

3.5 | RAW-Blue™ Assay

The biological activity of FI fractions was evaluated using the Raw Blue assay, which measures cellular response to lipopolysaccharide (LPS) stimulation in the presence of heparin-derived fractions. Absorbance values at 620/655 nm were recorded over a 4-h time course to assess the modulation of the inflammatory response by different fractions (Figure S10 and S11).

A similar trend was observed across all fractions, where cells treated with LPS alone exhibited the highest absorbance values, indicating a strong inflammatory response. In contrast, the addition of FI (Figure 3A) fractions reduced the absorbance, suggesting a dampening effect on LPS-induced stimulation. This effect was consistent across all fractions, implying that all fractions exerted some level of inhibition on LPS-induced activation.

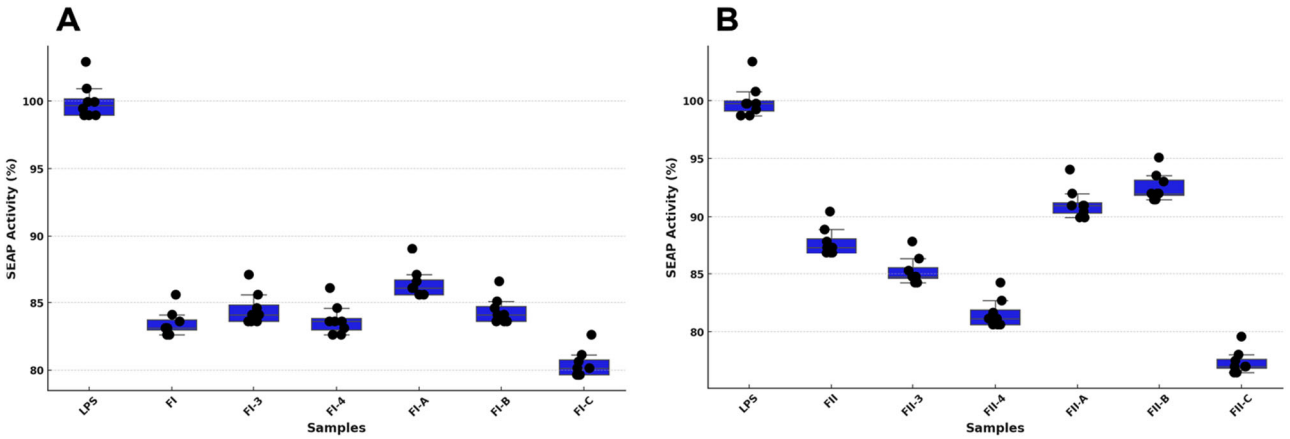

FIGURE 3 | Anti-inflammatory action of heparin byproduct fractions. (A) FI series (100 μg/mL), (B) FII (100 μg/mL) series. Activity is inferred from the alkaline phosphatase activity in the cell media. LPS serves as the control, with the corresponding absorbance value set at 100%. Data are presented as the average absorbance from 620 to 655 nm (5 nm increments), and the error bars depicted are standard deviations. End-point data (4 h) – see Figures S10 and 11 for the complete data set.

Likewise, a similar general trend was observed across all FII fractions (Figure 3B), where cells treated with LPS alone exhibited the highest absorbance values, indicating a strong inflammatory response. The addition of FII fractions reduced the absorbance, suggesting a dampening effect on LPS-induced activation. Notably, FII-C exhibited the most potent inhibitory effect, suggesting that its distinct GAG composition, higher sulfation degree, or molecular weight distribution may contribute to greater suppression of LPS-induced activation.

Given these observations and the contrasting structural characteristics - both substitution pattern and Mw - samples FII-A and FII-C were selected for further Raw Blue assays to determine whether pre-treating cells with heparin by-products had an effect (Figure 4). Cells pretreated with heparin 21 h before LPS addition demonstrated a markedly reduced response, suggesting that heparin modulates LPS-induced activation in a time-dependent manner.

These findings suggest that pretreatment with these fractions, despite their differences in composition and Mw, enhances the inhibitory effect on LPS-induced activation. This enhancement may occur by altering cellular receptor interactions or modulating intracellular signalling pathways over time, supporting the hypothesis that timing plays a crucial role in the ability of GAGs to suppress the inflammatory response. Thus, the mechanism of action is likely to involve early modulation of receptor interactions or intracellular signalling pathways, which become less accessible once LPS-induced activation is initiated or when exposure to inflammatory stimuli occurs shortly after GAG treatment.

3.6 | Peripheral Blood Mononuclear Cells (PBMCs) Ex Vivo Assay

IL-10 production was assessed following stimulation with distinct heparin fractions to evaluate their immunomodulatory effects. The results showed that cells treated with both by-product fractions exhibited an increase in IL-10 levels, indicating an anti-inflammatory response (Figure 5). However, this increase was lower than that observed with UFH, suggesting that while these fractions possess some immunomodulatory properties, their capacity to

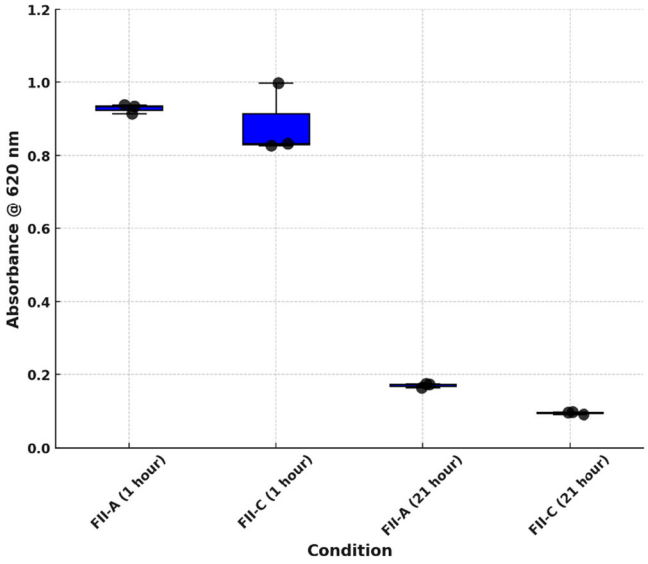

FIGURE 4 | The time-dependent anti-inflammatory action of fractions FII-A and C. Cells were pretreated with heparin fractions (100 μg/mL) for 1 or 21 h before exposure to LPS (10 ng/mL). Activity can be inferred from the alkaline phosphatase activity in the cell media. Data are presented as the average of 3 replicates, and the error bars depicted are standard deviations.

enhance IL-10 secretion is less pronounced compared to UFH. The control condition, in which cells were not exposed to GAG fractions, displayed low baseline IL-10 levels, confirming that the observed cytokine induction was a result of GAG stimulation rather than spontaneous production. These findings indicate that structural variations among the heparin fractions, including differences in GAG composition, sulfation degree and molecular weight, may play a crucial role in modulating IL-10 secretion.

4 | Discussion

This study provides a comprehensive structural and functional characterisation of GAG fractions derived from heparin production by-products, demonstrating how variations in sulfation,

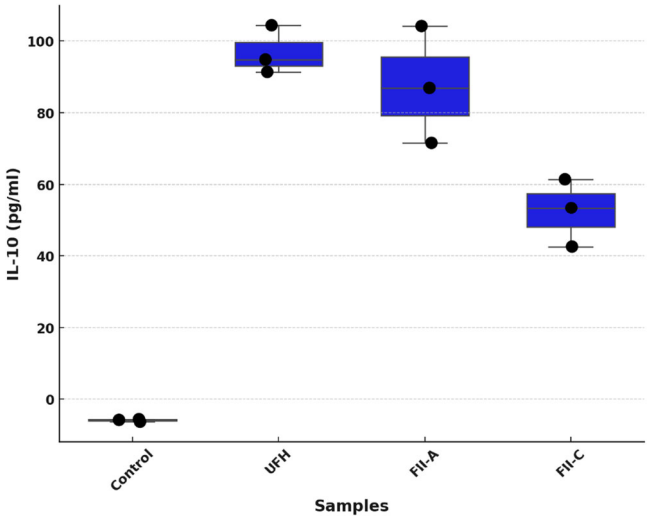

FIGURE 5 | Anti-inflammatory action of fractions FII-A and C on PBMCs ex vivo assay. IL-10 levels were measured after PBMCs activation and treatment with heparin and heparin byproduct fractions (100 μg/mL). Data are presented as the average of 3 replicates, and the error bars depicted are standard deviations. UFH, unfractionated heparin.

disaccharide composition, and molecular weight can influence their biological activity [19]. These fractions generated during heparin production exhibit potentially useful anti-inflammatory activities combined with low anticoagulant potential. Hence, they are existing reservoirs of potentially valuable pharmaceutical materials and have been produced under current regulatory frameworks.

Structural analyses using NMR and HP-SEC/TDA confirmed that both IEC and SEC fractionation effectively separated GAGs into distinct populations. The heparin-like fractions exhibited high levels of sulfation; some fractions displaying more highly sulfated IdoA2S-containing structures, presenting a more heparin-like character [20], while other fractions retained a more heterogeneous composition of HP/HS, DS, and CS. The variations in sulfation patterns and molecular weight suggest that these fractions are likely to display differential interactions with biological targets, particularly in modulating inflammatory responses [21].

The RAW-Blue™ assay demonstrated that heparin-derived fractions exert an inhibitory effect on LPS-induced NF-κB activation, suggesting their potential role as immunomodulatory agents. All fractions were capable of reducing the inflammatory response, though to varying degrees. Notably, FII-C exhibited the most potent inhibitory effect, implying that its higher sulfation degree, more heparin-like characteristic and specific molecular weight distribution may enhance its ability to modulate inflammatory signalling pathways. Further investigation into receptor-mediated interactions is warranted to understand whether these fractions influence TLR4 or other pattern recognition receptors involved in LPS-induced activation [22]. Additionally, the time-dependent nature of heparin by-product pretreatment was shown to significantly reduce LPS-induced activation. This highlights the importance of early intervention in inflammatory pathways which, similar to many cases involving the effect of heparin in signalling pathways [23], may include changes in receptor interactions or intracellular signalling pathways that alter the expression of cell-surface molecules acting as cell signalling centres [24].

The immunomodulatory properties of the heparin by-product fractions were further validated through the *ex vivo* PBMC assay, which assessed IL-10, a well-established anti-inflammatory cytokine [24], production following stimulation. Both fractions stimulated a measurable increase in IL-10 secretion, indicative of an anti-inflammatory response; however, the levels remained lower than those induced by UFH. This suggests that while these fractions retain some immunomodulatory potential, structural variations such as saccharide composition, substitution pattern and molecular weight may influence their capacity to enhance regulatory cytokine production [21].

Notably, these fractions are derived from heparin production by-products, which are known to exhibit negligible anticoagulant activity [10, 21]. This characteristic is particularly beneficial, as it suggests that, despite their lower potency compared to UFH, these fractions may exert fewer off-target effects, reducing the risk of unwanted anticoagulation and bleeding [25]. Additionally, their repurposing contributes to the valorisation of heparin manufacturing waste, aligning with circular economy principles, enhancing resource efficiency and directly supporting the United Nations SDGs by promoting waste reduction and sustainable bioprocessing [26].

Together, these findings highlight the potential of heparin by-products as bioactive molecules capable of influencing inflammatory pathways. The observed structural and functional differences among the fractions underline the importance of sulfation patterns and molecular weight in modulating biological activity [9, 19]. While UFH remains the most potent modulator of IL-10 production, by-product fractions show promise as alternative therapeutic candidates. Further studies should focus on determining the interactions at the molecular and signalling network level responsible for their immunomodulatory effects and assessing their potential applications in inflammation-related disorders.

Author Contributions

Emilia Uslenghi: conceptualization, investigation, writing – original draft, methodology; **Taran Kandola:** conceptualization, investigation, writing – original draft, methodology, validation; **Sofia Nizzolo:** conceptualization, investigation, methodology; **Ethan Saunders:** methodology, investigation; **Tye Gee Jun:** investigation, methodology, resources; **Mark A. Skidmore:** investigation, funding acquisition, methodology; **Edwin A. Yates:** conceptualization, writing – original draft, validation, writing – review and editing, formal analysis, resources, supervision; **Marco Guerrini:** conceptualization, investigation, funding acquisition, writing – review and editing, resources, methodology, supervision; **Marcelo A. Lima:** conceptualization, investigation, funding acquisition, writing – original draft, methodology, writing – review and editing, formal analysis, project administration, data curation, supervision, resources; **Antonella Bisio:** conceptualization, investigation, funding acquisition, writing – original draft, writing – review and editing, methodology, formal analysis, project administration, supervision, data curation, resources.

Acknowledgments

MAL thanks the Royal Society (IEC\NSFC\201116), the Academy of Medical Sciences/Wellcome Trust (Springboard grant, SBF007\100054), EPSRC (EP/X019179/1), and Ronzoni Foundation. Dr. Michela Parafioriti is thanked for assistance in generating NMR figures.

Conflicts of Interest

The authors declare no conflicts of interest.

Data Availability Statement

The data sets generated and analysed during this study are available from the corresponding author upon reasonable request.

References

1. R. Simmons, N. Culkin, and V. Davies, "Crisis Resilient Supply Chain Design - Post Pandemic, Post Ukraine Conflict Challenges and Opportunities," *SSRN Electron J* (2022), https://doi.org/10.2139/ssrn.4099642.

2. M. C. Z. Meneghetti, A. J. Hughes, T. R. Rudd, et al., "Heparan Sulfate and Heparin Interactions With Proteins," *Journal of the Royal Society Interface* 12 (2015): 20150589, https://doi.org/10.1098/rsif.2015.0589.

3. M. Guerrini, P. A. J. Mourier, G. Torri, and C. Viskov, "Antithrombin-Binding Oligosaccharides: Structural Diversities in a Unique Function?," *Glycoconjugate Journal* 31 (2014): 409–416, https://doi.org/10.1007/s10719-014-9543-9.

4. S. T. Olson, B. Richard, G. Izaguirre, S. Schedin-Weiss, and P. G. W. Gettins, "Molecular Mechanisms of Antithrombin–Heparin Regulation of Blood Clotting Proteinases. A Paradigm for Understanding Proteinase Regulation by Serpin Family Protein Proteinase Inhibitors," *Biochimie* 92 (2010): 1587–1596, https://doi.org/10.1016/j.biochi.2010.05.011.

5. L. Wang, J. R. Brown, A. Varki, and J. D. Esko, "Heparin's Anti-Inflammatory Effects Require Glucosamine 6-O-sulfation and Are Mediated by Blockade of L- and P-Selectins," *Journal of Clinical Investigation* 110 (2002): 127–136, https://doi.org/10.1172/JCI14996.

6. C. J. Mycroft-West, D. Su, I. Pagani, et al., "Heparin Inhibits Cellular Invasion by SARS-CoV-2: Structural Dependence of the Interaction of the Spike S1 Receptor-Binding Domain With Heparin," *Thrombosis and Haemostasis* 120 (2020): 1700–1715, https://doi.org/10.1055/s-0040-1721319.

7. J. A. Tree, J. E. Turnbull, K. R. Buttigieg, et al., "Unfractionated Heparin Inhibits Live Wild Type SARS-CoV-2 Cell Infectivity at Therapeutically Relevant Concentrations," *British Journal of Pharmacology* 178 (2021): 626–635, https://doi.org/10.1111/bph.15304.

8. A. K. Kakkar and F. Macbeth, "Antithrombotic Therapy and Survival in Patients With Malignant Disease," *British Journal of Cancer* 102 (2010): S24–S29, https://doi.org/10.1038/sj.bjc.6605602.

9. D. Xu and J. D. Esko, "Demystifying Heparan Sulfate–Protein Interactions," *Annual Review of Biochemistry* 83 (2014): 129–157, https://doi.org/10.1146/annurev-biochem-060713-035314.

10. S. L. Taylor, J. Hogwood, W. Guo, E. A. Yates, and J. E. Turnbull, "By-Products of Heparin Production Provide a Diverse Source of Heparin-Like and Heparan Sulfate Glycosaminoglycans," *Scientific Reports* 9 (2019): 2679, https://doi.org/10.1038/s41598-019-39093-6.

11. G. Cassinelli and A. Naggi, "Old and New Applications of Non-Anticoagulant Heparin," *International Journal of Cardiology* 212 (2016): S14–S21, https://doi.org/10.1016/S0167-5273(16)12004-2.

12. UN General Assembly, Transforming Our World: the 2030 Agenda for Sustainable Development. Available: https://www.refworld.org/legal/resolution/unga/2015/en/111816.

13. B. E. Fan and E. J. Favaloro, "Counting the Carbon Cost of Heparin: an Evolving Tragedy of the Commons?," *Lancet Haematology* 9 (2022): e469–e471, https://doi.org/10.1016/S2352-3026(22)00171-5.

14. S. E. Sivinski, L. K. Mamedova, R. A. Rusk, et al., "Development of an In Vitro Macrophage Screening System on the Immunomodulating Effects of Feed Components," *Journal of Animal Science and Biotechnology* 11 (2020): 89, https://doi.org/10.1186/s40104-020-00497-4.

15. L. Mauri, M. Marinozzi, G. Mazzini, et al., "Combining NMR Spectroscopy and Chemometrics to Monitor Structural Features of Crude Heparin," *Molecules* 22 (2017): 1146, https://doi.org/10.3390/molecules22071146.

16. E. Vismara, M. Pierini, G. Mascellani, et al., "Low-Molecular-Weight Heparin From Cu2+ and Fe2+ Fenton Type Depolymerisation Processes," *Thrombosis and Haemostasis* 103 (2010): 613–622, https://doi.org/10.1160/TH09-02-0084.

17. S. Bertini, A. Bisio, G. Torri, D. Bensi, and M. Terbojevich, "Molecular Weight Determination of Heparin and Dermatan Sulfate by Size Exclusion Chromatography With a Triple Detector Array," *Biomacromolecules* 6 (2005): 168–173, https://doi.org/10.1021/bm049693s.

18. A. I. K. Abdo, F. Nordin, and G. J. Tye, "Selection and Evaluation of Single Domain Antibody Against p19 Subunit of IL-23 by Phage Display for Potential Use as an Autoinflammatory Therapeutic," *International Immunopharmacology* 137 (2024): 112371, https://doi.org/10.1016/j.intimp.2024.112371.

19. O. A. Wilkinson and M. C. Fernig, "DG. The Heparanome and Regulation of Cell Function: Structures, Functions and Challenges," *Frontiers in Bioscience* 13 (2008): 4309–4338, https://doi.org/10.2741/3007.

20. S. F. Chavante, A. S. Brito, M. Lima, et al., "A Heparin-Like Glycosaminoglycan From Shrimp Containing High Levels of 3-O-sulfated D-Glucosamine Groups in an Unusual Trisaccharide Sequence," *Carbohydrate Research* 390 (2014): 59–66, https://doi.org/10.1016/j.carres.2014.03.002.

21. N. Veraldi, A. J. Hughes,T. R. Rudd, et al., "Heparin Derivatives for the Targeting of Multiple Activities in the Inflammatory Response," *Carbohydrate Polymers* 117 (2015): 400–407, https://doi.org/10.1016/j.carbpol.2014.09.079.

22. A. Ciesielska, M. Matyjek, and K. Kwiatkowska, "TLR4 and CD14 Trafficking and Its Influence on LPS-Induced Pro-Inflammatory Signaling," *Cellular and Molecular Life Sciences* 78 (2021): 1233–1261, https://doi.org/10.1007/s00018-020-03656-y.

23. J. H. Lee, J. Lee, G. H. Seo, C. H. Kim, and Y. S. Ahn, "Heparin Inhibits NF-κB Activation and Increases Cell Death in Cerebral Endothelial Cells After Oxygen-Glucose Deprivation," *Journal of Molecular Neuroscience* 32 (2007): 145–154, https://doi.org/10.1007/s12031-007-0026-3.

24. S. Laner-Plamberger, M. Oeller, R. Poupardin, et al., "Heparin Differentially Impacts Gene Expression of Stromal Cells From Various Tissues," *Scientific Reports* 9 (2019): 7258, https://doi.org/10.1038/s41598-019-43700-x.

25. M. Lima, T. Rudd, and E. Yates, "New Applications of Heparin and Other Glycosaminoglycans," *Molecules* 22 (2017): 749, https://doi.org/10.3390/molecules22050749.

26. M. Sarkis, A. T. Fyfe, C. Kontoravdi, and M. M. Papathanasiou, "Towards a Net Zero, Socially Sustainable and Eco-Efficient Biopharma Industry: How Far Are We?," *Current Opinion in Chemical Engineering* 44 (2024): 101027, https://doi.org/10.1016/j.coche.2024.101027.

Supporting Information

Additional supporting information can be found online in the Supporting Information section.